Comparison of RADARSAT imaging modes to monitor land use in coastal areas

Nathalie Beaulieu, Grégoire Leclerc and William Bell,
Centro Internacional de Agricultura Tropical (CIAT),
AA6713, Cali Columbia. E-mail: n.beaulieu@cgnet.com
Daniel Marmillod, Centro Agronómico Tropical de Investigación y Enseñanza (CATIE), Costa Rica,
Christian Asch Quirós, Instituto Geográfico Nacional (IGN), Costa Rica
Dirk Werle, AERDE Environmental Research, Halifax, NS, Canada.

Abstract

We present preliminary results obtained from studying RADARSAT imagery to monitor land use at two coastal sites in Central America, one in Pacific northern Nicaragua, the other in Pacific southern Costa Rica. The scope of this paper is to compare the ability of different imaging modes to evidence land use features in the mangroves and their surroundings. In the Nicaraguan site, we qualitatively compare images acquired with similar resolutions but with different incidence angles, modes S1, S7 and EH5. In the Costa-Rican site, we compare the fine mode F5 and the standard mode S1 in terms of their information content and on the effect of speckle filtering on the effective number of looks. An obvious result is that the monitoring of aquaculture activities and river dynamics is a promising application for all modes under study, although the sensitivity of lower incidence angles to wind roughened water makes mode S1 less suitable for an automatic separation of water surfaces. In the Nicaraguan site, the S1 mode showed less contrast between agricultural bare fields and forest than did modes S7 and EH5. All three modes were sensitive to the presence of low shrubs on the extensive mudflats in that site. Fine mode imagery allowed the detection of street patterns in urban areas and to some extent narrow tree lines, while standard modes didn't. In the Costa-Rican site, S1 produced more pronounced tonal variations between low and high mangrove stands than the F5 image. However, the higher resolution and higher incidence angle of the F5 image produced clearer highlights and shades at the limits between stands of different heights and allowed a better identification of narrow water channels than did the S1 image.

1. Introduction

This study encompasses a series of RADARSAT images acquired over two coastal sites in Nicaragua and Costa Rica, which were part of the Canadian Space Agency's ADRO program. The study's aim is to demonstrate RADARSAT's utility for monitoring land use and to compare different acquisition modes in terms of their ability to evidence certain features in mangroves and their surroundings. The Nicaraguan site covers the area surrounding the Estero Real estuary, an affluent to the Fonseca Gulf, near the border with Honduras. The main issues in this area include the planning of aquaculture to mitigate impact on mangroves, and the planning of land use with the objective of reducing sediment load to the estuaries. In the following sections, we will simply refer to this site as "Estero Real". We must mention that the Fonseca Gulf is shared between three countries, Nicaragua, Honduras and El Salvador, and is the focal point of various sustainable development projects. The Costa-Rican site is located to the North of the Osa peninsula, to the South-west of the country, and encompasses the area of influence of the Térraba and Sierpe estuaries. It is referred to as the "Térraba-Sierpe" site. The mangroves of this site are much more continuous than in Estero Real; they also harbor aquaculture activities, but to a lesser extent. In both sites, the presence of banana plantations and other intensive agriculture could be affecting the ecology of the mangroves. For these two sites we count on field data, topographic maps at 1:50,000 scale, complementary optical imagery and, in the case of Térraba-Sierpe, airborne SAR images. Both of these sites have been under study by the *DANIDA/Manglares* project and by the *Proyecto para el Desarrollo Sostenible en América Central*

2. Description of imagery and ancillary data

The RADARSAT images were acquired in ascending mode in May, 1996, and delivered the following September in 16-bit unsigned format as "Path Image Plus" products. Table 1 shows a summary of the characteristics of these images, as well as other images used for comparison purposes.

In the case of the Estero Real site, ground reference data was collected in the field by CATIE's DANIDA/Manglares project a month before the images were acquired. A SPOT panchromatic image of the area, acquired two months before the RADARSAT images, is also used as reference data. In the case of Térraba-Sierpe in Costa Rica, the RADARSAT images were referenced to a digital geographic database elaborated from 1987 panchromatic 1:20000 scale aerial photographs and ground surveys (Asch Quiros, 1993). For this site, we are also using a 1994 Landsat TM image and a high-resolution airborne C-band image, acquired in 1992 in the scope of the SAREX'92 mission (Wooding and Zmuda, 1994) and Proyecto Radar Costa Rica/Canada.

Table 1: Summary of characteristics of RADARSAT and other images used in this study

Sensor	Mode	Resolution (m) range	azm.	pixel spacing (m) range	azm.	incident angle (°) nr	fr	band, polariz.	nominal n. looks	date	site	Project
CCRS C-X SAR	wide swath	20	10	15	6.9	45	85	C-HH, C-VV	7	27/04/92	Térraba Sierpe	SAREX 92-Proy.Radar Costa Rica/Canada
RADARSAT	Fine 5	10	9	3.125	3.125	45	48	C-HH	1	09/05/96	Térraba Sierpe	ADRO
RADARSAT	Standard 1	26	27	8	8	20	27	C-HH	4	13/05/96	Térraba Sierpe	ADRO
Landsat TM	Multispectral			28.5	28.5	-	--	7-V,IR	--	3/09/94	Térraba Sierpe	REFORMA
RADARSAT	Extended H 5	18.2	27	8	8	56	58	C-HH	1	23/05/96	Estero Real	ADRO
RADARSAT	Standard 7	20.09	27	8	8	45	49	C-HH	1	13/05/96	Estero Real	ADRO
RADARSAT	Standard 1	26	27	8	8	20	27	C-HH	4	15/05/96	Estero Real	ADRO
SPOT XS	Multispectral			20	20	-	--	3-V,IR	--	25/02/96	Estero Real	DANIDA/Manglares

3. The Estero Real site

For this site, we visually compare modes with similar resolutions but different incident angles: modes Standard 1 (S1), Standard 7 (S7) and Extended 5 (EH5). The three images are compared to one another using the SPOT image and ground survey data as a reference. The images were georeferenced and overlaid with the SPOT image in a UTM projection, with an output pixel spacing of 20m, using a cubic convolution resampling, a linear transformation and ground control points collected from streams digitized from 1:50,000 scale topographic maps. Figures 1a) and 2a) show subsets of the radar color composite displaying S7 in red, S1 in green and EH5 in blue. Figures 1b) and 2b) show the same coverage in the SPOT image, bands 3, 2, 1 displayed in red, green and blue, respectively.

Figure 1: Close-up on a mangrove area with agriculture to the South. a) RADARSAT color composite S7, S1, EH5 in RGB. b) Same area in SPOT color composite, bands 3, 2, 1 in RGB.
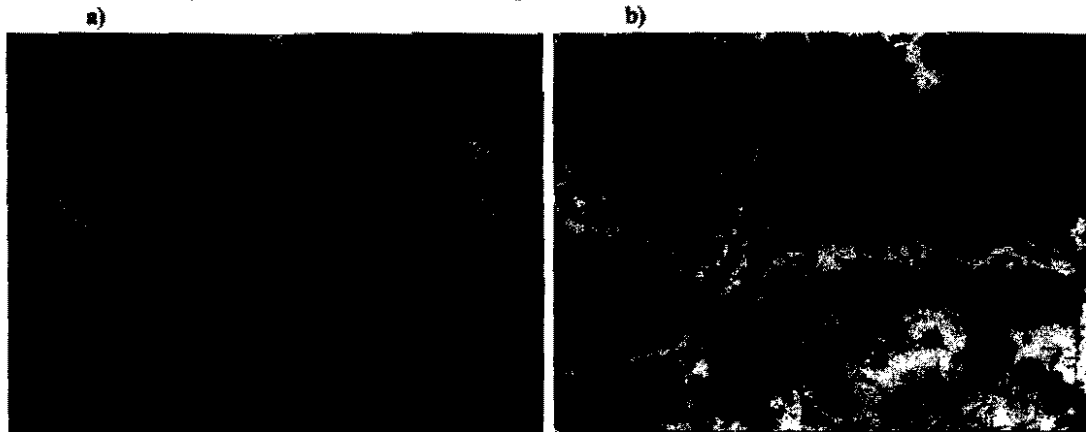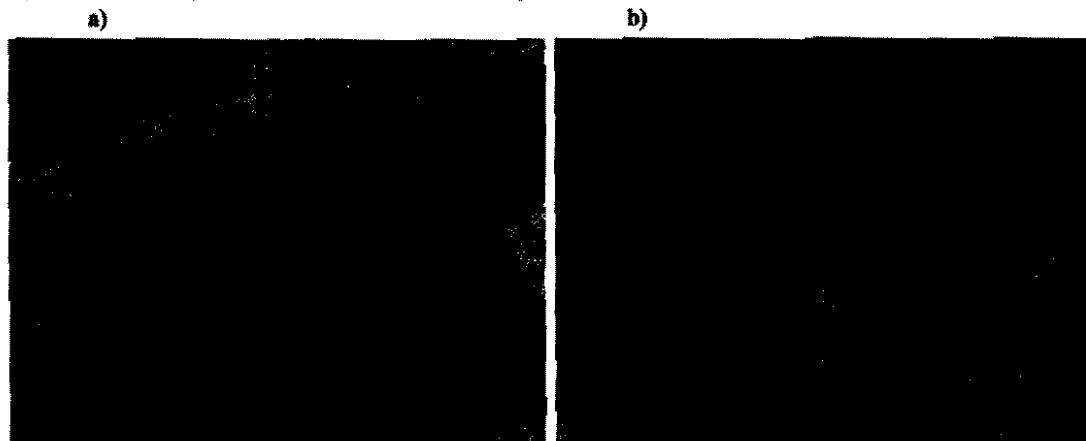
a)   b)

Figure 2: Close-up on the estuary, mangroves and aquaculture ponds. a) RADARSAT color composite S7, S1, EH5 in RGB. b) Same area in SPOT color composite, bands 3, 2, 1 in RGB.

a)   b)

3.1 Visual Interpretation

The most apparent difference between the RADARSAT modes is that the S1 (green) is more sensitive to water surface roughness, as can be seen in the estuary and in the Fonseca Gulf on the upper left corner of figure 2 a). S1 also produces brighter tones than the two other modes in the bare soil areas, which are characterized by light green, beige, light blue or white in the SPOT subsets. Sediment yield from the watershed is one of the processes that most affect mangroves. The identification of sediment sources such as bare fields at the beginning of the rainy season is an important issue that is difficult to address with remote sensing images in the optical domain, because of cloud cover. The fact that the S1 mode produced relatively high backscatter for bare soils makes it less suitable to pick out bare agricultural fields. The S1 image showed no significant difference in tone between a large extension of bare cotton fields and adjacent areas with mixed vegetation, whereas S7 and EH5 were more contrasted in these areas, allowing an easy identification of the bare fields. These fields appear dark in the S7 and EH5 images, and produce greenish tones near the lower right portion of the color composite of figure 1 a).

As can be seen on figure 2b), the Estero Real site is characterized with mangrove tree vegetation (red) on

the banks of the streams which are separated by mudflats. These mudflats are partly colonized by varying densities of shrubby vegetation. They appear in bluish and brownish tones on the SPOT image, depending on the density of the shrubby vegetation and on the moisture of the soil. These areas are flooded with a frequency that depends on their altitude. The RADARSAT color composite (figure 2a), shows a great sensitivity to the shrubby vegetation on these mudflats, much more clearly than on the SPOT image. A clear identification of the shrubby vegetation coverage seems, however, to be much more difficult with the S1 mode than with the two other modes, because of high backscatter in bare soil and wind-roughened water. Identification of extensions of low shrubs in the mudflats of the Estero Real is a crucial issue. In certain areas, these are thought to be regenerating forest. These extensions of shrubby vegetation do not appear on the maps used for planning of aquaculture concessions. Although law protects mangrove vegetation, the distribution of this shrubby vegetation is not well known and its presence is often not taken into account.

However, the variations of height, density and species in the tree vegetation do not produce significant variations of tone in any of the three RADARSAT modes. This is most apparent in figure 2, where taller Rhizophora dominated stands (bright red on the SPOT composite), shorter and dull-green leaved Avicennia (dark reddish brown on the SPOT composite) and shrub-covered mudflats (varying shades of light brown on light blue) produce similar pink tones on the radar composite. The next step will be to integrate radar with SPOT to improve a classification which the CATIE's DANIDA/Manglares project has recently conducted over the area using SPOT alone.

Another interesting feature is that the EH5 mode (which corresponds to the highest incidence angle) showed brighter tones than the other two modes for scrubland and certain agricultural fields, which appear in bluish tones on the RADARSAT composite. EH5 and S7 showed better contrasts between banana plantations and their surroundings, although they still appear distinctively bright on the S1 image. The identification of banana plantations is another application for which RADARSAT can advantageously complement optical domain imagery.

The utility of RADARSAT imagery for the delineation of shrimp ponds, estuaries and natural lagoons is indisputable for all acquisition modes. The mapping and monitoring of shrimp ponds is of primary importance, as these are sometimes illegally established or enlarged before permits are solicited. The natural lagoons in Nicaragua's Estero Real are traditionally exploited by the local population for shrimp gathering, and are respected as such by the government. Proper mapping of these lagoons can avoid conflicts resulting from planning commercial shrimp exploitation in these areas by mistake. The embankments between artificial shrimp ponds appear more clearly in the S1 image than in the other two modes.

4. Térraba Sierpe.

For the Térraba-Sierpe site, we compare images of different spatial resolutions for their ability to evidence certain features in the mangroves and their surroundings, images acquired in modes fine F5 and standard S1. Variation of the antenna gain caused by the automatic gain control used at the time of the acquisition of the images, which was affected by the shape of the coastline, prevented any attempt at calibration. The acquisition of a standard mode S7 image was twice planned over the area but its processing failed both times. It will be reacquired to allow the comparison of the S1 and S7 modes for this site also.

4.1 Image preprocessing.

Since the studied images are Path Image Plus products (pixel much smaller than resolution), both S1 and F5 imagery contain substantial autocorrelation, which shows as a granular texture about 4 pixels wide. Analysis of the semivariogram for homogeneous areas showed spatial correlation up to a distance of 4 pixels, with no spatial correlation for larger distances. Although the high sampling density of these products

has its purpose and allows better mapping of point and line objects, we block-averaged the imagery in order to obtain a speckle with low autocorrelation, on which speckle filters function better.

Figure 3 shows 512x512 pixel subsets of the images, and figure 4 shows subsets of the same number of pixels for the image averaged with 3x3 blocks. The effective number of looks was calculated for homogeneous areas on the original images and on the images averaged with 2x2 and 3x3 blocks. The effective number of looks, n_{look}, is calculated from the average brightness power $\overline{P}$ and the standard deviation of the power, $std(\overline{P})$, in the following manner:

$$n_{look} = \sqrt{\frac{\overline{P}}{std(\overline{P})}} \qquad \text{where} \qquad std(\overline{P}) = \sqrt{\overline{P^2} - \overline{P}^2}$$

While the nominal number of looks is 1 for the fine mode and 4 for the standard, the average effective number of looks for the original 16 bit imagery was 0.97 for F5 and 3.3 for S1, as computed from areas of banana and rice. For the 3x3 block-averaged images, these numbers rise to 1.85 for F5 and 4.56 for S1. This small increase may suggest that the information content of the original imagery is not substantially altered by block averaging, while the size of the imagery is drastically reduced. Regarding spatial correlation for Path Image Plus imagery, 3x3 block averaging showed to be optimum and was chosen as the basis for further processing. It results in images with a pixel spacing of 9.375 m in fine mode and 24 m in standard mode.

Figure 3: Subset of mixed uses area. Original imagery:
       a) fine F5 mode: b) standard S1 mode
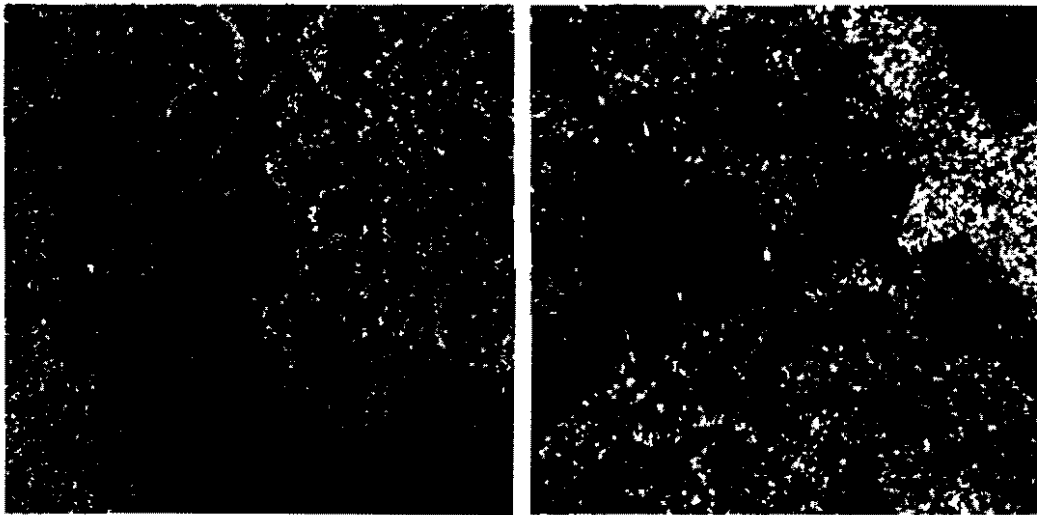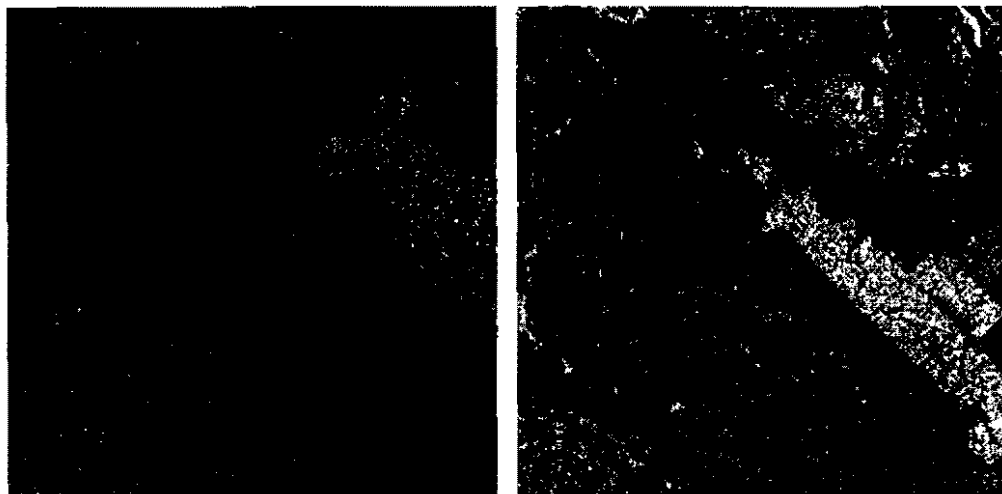
Figure 4: Subset of mixed uses area. 3x3 block-average of original imagery:
a) fine F5 mode   b) standard S1 mode

4.2 Filtering and image quality

Sixteen bit imagery were filtered using the Gamma MAP filter using both 3x3 and 5x5. This convolution filter is an adaptation by Lopes *et al.* (1993) of Kuan's MAP filter. It assumes a gamma distribution for speckle, and thus requires *a priori* knowledge of the speckle statistics. In addition, two thresholds are defined to decide how to modify the value of the filtered pixel, on the basis of the coefficient of variation. This filter is implemented in the PCI radar module (FGAMMA.EXE, PCI, 1996). We used the average number of looks obtained for rice and bananas in the 3x3 block-averaged image as an input to the Gamma MAP filtering procedure. The effect of the application of a 5x5 window Gamma Map filter on the subsets of figure 4 is shown in figure 5. We also used a Geometric filter (Lira *et al.*, 1993, see description in Appendix) on the 3x3 block-averaged imagery scaled to 8 bits, trimming the lower end of the histogram by 0.5% and the upper end by 3.5% to improve contrast in the studied area, to the detriment of contrast in the high relief areas. This produced a well-balanced histogram but slightly distorted the intensity-speckle ratios and therefore altered the number of looks. The Geometric filter erodes speckle slowly and several passes were necessary to produce speckle-free images. Although much slower, it produced a better visual aspect than the Gamma MAP filter which left the filtered imagery with annoying "ripples" and bright spots.

Figure 5: Subset of mixed uses area. 3x3 block average of original imagery filtered by 5x5 Gamma MAP filter: a) fine F5 mode, n_{look} (unfiltered) =1.85   b) standard S1 mode, n_{look} (unfiltered) =4.56
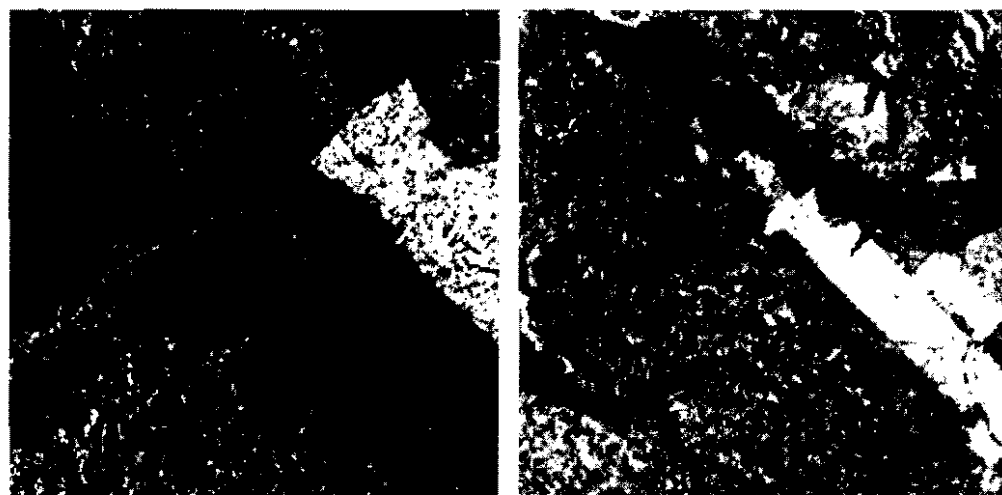
Figure 6: Subset of mixed uses area. 3x3 block average of original imagery, scaled to 8 bits: 5 passes of the Geometric filter.

a) fine F5 mode   b) standard S1 mode
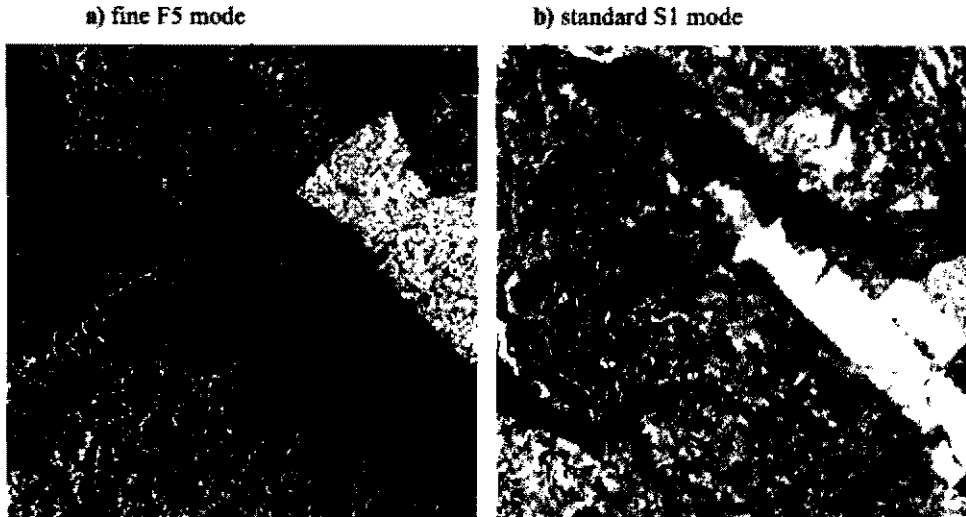
Figures 7 and 8 show the evolution of the effective number of looks with different processing steps, respectively for modes F5 and S1. For both these figures, frame a) illustrates the effect of block averaging and application of the Gamma filter on the 3x3 block-averaged 16 bit imagery, while frame b) illustrates the effect of different numbers of passes of the geometric filter on the images scaled to 8 bits. We notice that the effective number of looks increases very little with 2x2 or 3x3 block-averaging, but does increase significantly with filtering of the 3x3 block-averaged images, except for aquaculture in the S1 image. For S1 imagery, aquaculture areas showed unusually low quality factors (number of looks below 1), which did not increase through filtering. This is caused by the texture corresponding to uneven water roughness. The S1 image is more sensitive to water roughness than the F5 image acquired with a higher incident angle, similarly to what was observed for the Estero Real site. We notice that the application of four and five passes of the Geometric filter produced a higher number of looks for aquaculture than did the Gamma MAP filter. This increase in homogeneity would be useful for the automatic segmentation of water surfaces.

Figure 7: Effect of different processing steps on the effective number of looks for the F5 image.
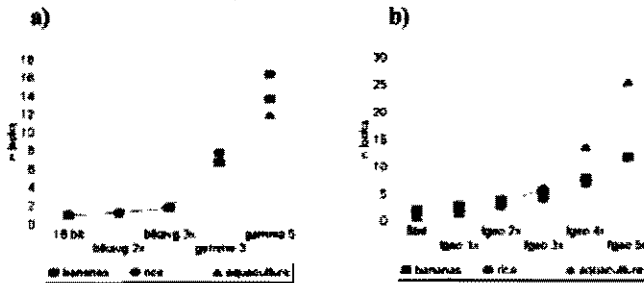
Figure 8: Effect of different processing steps on the effective number of looks for the S1 image.
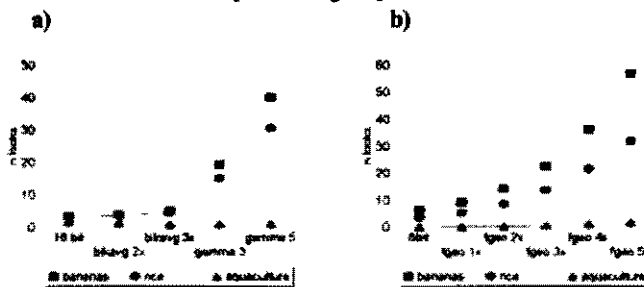
4.3 Visual Interpretation

Filtered and unfiltered imagery were studied visually by overlaying the land use and vegetation maps of the area. Only preliminary observations are made here.

We noticed that patches of mangrove fern areas (Acrostichum aureum) produced a darker tone in both images. The S1 image seemed to produce more difference in tone between higher and lower stands of forest or Acrostichum aureum. Neither RADARSAT mode showed significant visual texture within the high mangrove forest. However F5 allowed the delineation of high and low mangrove forest boundaries. In comparison, the airborne SAR image, with a resolution almost comparable to RADARSAT's fine mode but with 7 looks, showed many interesting textural features. For example, it allowed the discrimination of Pelliciera sp. patches within dominant Rhizophora sp. forest as well as clear highlights and shades where there were mangrove stands of varying height. Mougin et al. (1994) found that the use of radiometric and textural parameters derived from high-resolution (6 m x 6 m) airborne images from the SAREX'92 mission could help distinguish mangrove types and general growth stages. They do not report results with C-HH, but in C-VV they found that young and decaying mangroves exhibited stronger backscatter than mature mangroves.

Banana plantations show noticeable high brightness while rice fields appear relatively dark at this period of the year in the RADARSAT images. Pasture areas show similar and darker tones. Urban areas were well defined on the F5 image, but produced randomly distributed bright spots on the S1 image. Block-averaging did not seem to significantly affect the suitability of the images for mapping estuaries, channels and aquaculture , but certain narrow boundaries between the artificial ponds only appeared on the original F5 imagery. The S1 image was very sensitive to water roughness, which is observable even within aquaculture ponds.

We have created a georeferenced dataset with a 10x10 m pixel grid where the Landsat TM, airborne C-HH, RADARSAT images and a photointerpreted vegetation map have been combined. We are currently studying how different RADARSAT modes can be combined with other imagery to improve interpretability of land use classes and will soon be evaluating the S7 mode. We do know that reprocessing will be necessary for our F5 mode image, which shows strong signal increase from far to near range, and varying gain in the azimuth direction due to effect the shape of the coastline on the automatic gain control used during acquisition of earlier RADARSAT images.

5. Conclusions

For the Estero Real site, we observed that the higher incident angle modes, S7 and EH5, were more suitable to distinguish bare soil from vegetated areas because of their darker tone, whereas in the S1 mode bare soil fields often appeared relatively bright. S7 and EH5 also seem more suitable for mapping the distribution of shrubs in the mudflats, because S1 showed bright tones for wind roughened water and sometimes on the bare mudflats themselves. The next step for the Estero Real site will be to combine RADARSAT and SPOT to improve a classification that has recently been conducted by the DANIDA/Manglares project, based on the SPOT image and ground surveys.

For the Térraba-Sierpe site, the fine mode imagery F5 did not seem to offer major advantages over the standard mode S1 in terms of forest texture and distinction between land cover types. However, it allowed a better detection of urban areas, of small streams and channels, of limits between agricultural fields, of embankments between aquaculture ponds, and allowed the delineation of narrow channels and boundaries between some forest stands of different heights. S1 imagery showed appreciable tonal variations in the mangrove area, which should allow mapping of some very general vegetation classes.

RADARSAT images can advantageously complement optical imagery for the mapping of low shrubby vegetation, as is the case in Estero Real. The monitoring of aquaculture is a promising application for all modes under study. More research is currently being done on the two data sets, and we hope to be able, in

the near future, to draw more detailed conclusions on the applicability of RADARSAT acquisition modes.

For the interpretation of land use and vegetation, the RADARSAT Path Image Plus product was found to have an unnecessarily high sampling density; presenting a speckle with grains composed of various pixels (spatial correlation extends up to 4 pixels), making the images difficult to filter. Files are huge (nominally 512 MB for the fine mode, 313 MB for standard mode) making handling difficult by users with software or hardware limitations. Files can be transformed into a more widely useable form by scaling to 8 bits and block averaging. We found that a 3x3 block averaging produced no substantial loss in image interpretability. Another advantage is that scaling to 8-bit and 3x3 block-averaging produces files which are 18 times smaller than the original. The Geometric filter described in appendix gave excellent results and compared favorably to the Gamma MAP filter.

6. References

Asch Quirós, C. (1993). Estudio de Fotointerpretación y confección de mapas de uso de la tierra y unidades vegetativas de la reserva forestal Térraba-Sierpe y zonas aledañas. Informe, Proyecto Danida/Manglares. Centro Agronómico Tropical de Investigación y Enseñanza (CATIE).

Lira, J, Fernández, S., and Moreno, V. (1993). Análisis de texturas en Imágenes SAR. Seminario Internacional de Radar, San Jose, Costa Rica, 1-5 November 1993. Instituto Geográfico Nacional de Costa Rica.

Lopes, A., Nezry, E., Touzi, R., and. Laur, H. (1993). Structure detection and statistical adaptive speckle filtering in SAR images. International Journal of Remote Sensing, Vol. 14, No. 9, p. 1735-1758.

Mainardi, V. (1996). El manglar de Térraba-Sierpe en Costa Rica. Serie técnica, Informe Técnico No. 284. Proyecto Conservación para el Desarrollo Sostenible en América Central (OLAFO), CATIE. 91 p.

Mougin, E., Lopes, A., Hery, P., Marty, G., Le Toan, T., Fromard, F., Rudant, J.P. (1994). Multifrequency and multipolarization observations on mangrove forests of French Guyana during SAREX'92 experiment, preliminary results. Workshop proceedings, SAREX'92 South America Radar Experiment, ESA, Paris, 6-8 December 1993. ESA WPP-76, p. 193-204.

PCI, Inc. (1996). EASI/PACE technical reference, version 6.01, Richmond Hill, Canada.

Pratt, W.K. (1991). Digital image processing. Wiley Interscience, New York, USA.

Wooding, M. G. and Zmuda, A. D. (1994). An overview of SAREX-92 data acquisition and analysis of the tropical forest environment. Workshop proceedings, SAREX'92 South America Radar Experiment, ESA, Paris, 6-8 December 1993. ESA WPP-76, p. 3-14.

APPENDIX: Description of the geometric filter used in this study.

The geometrical filter is an edge-preserving morphological speckle filter for 8-bit radar data. It has originally been described by Lira *et al.* (1993). It can be applied several times if the speckle is strong.

Algorithm

Reduction of speckle with the Geometric Filter is achieved based on the morphological operation Intersect-No-Intersect, which is equivalent to an erosion-dilatation operation (Pratt, 1991). The first requirement for the optimal use of this filter is that the speckle's autocorrelation function decreases rapidly, reaching a value of zero (ideally) after the nearest neighbors. This allows the application of morphological operations within a window 3 pixels wide. The second requirement is that the field of the image be stationary. Finally noise and signal have to be decorrelated, which implies that the speckle is generated independently for each pixel.

Operation of this filter can be visualized as follows: for a given image, a profile is read in the 4 directions horizontal, vertical, diagonal and backdiagonal. For each direction, one constructs two binary profiles of the digital number, the points corresponding to null values:

```
255 |  . . . . . . 1 . . . . . . . . . . . . . . . . . . . . . . . . . . . . . . .
    |  1 . . . . 1 . . . . . . 1 . . . . . 1 . . . . . . 1 . . . . . . 1 1 1 .
DN  |  1 1 . . 1 1 1 . . . 1 1 . 1 . 1 . 1 1 1 1 1 . 1 . 1 1 . 1 . 1 1 1 1 1
    |  1 1 1 1 1 1 1 1 1 1 1 1 1 1 1 1 1 1 1 1 1 1 1 1 1 1 1 1 1 1 1 1 1 1 1 1 1
    |  1 1 1 1 1 1 1 1 1 1 1 1 1 1 1 1 1 1 1 1 1 1 1 1 1 1 1 1 1 1 1 1 1 1 1 1 1
  0 |  1 1 1 1 1 1 1 1 1 1 1 1 1 1 1 1 1 1 1 1 1 1 1 1 1 1 1 1 1 1 1 1 1 1 1 1 1
              pixel along profile
```

and its complement:

```
255 |  1 1 1 1 1 1 1 1 1 1 1 1 1 1 1 1 1 1 1 1 1 1 1 1 1 1 1 1 1 1 1 1 1 1 1 1 1
    |  1 1 1 1 1 . 1 1 1 1 1 1 1 1 1 1 1 1 1 1 1 1 1 1 1 1 1 1 1 1 1 1 1 1 1 1 1
DN  |  . 1 1 1 1 . 1 1 1 1 1 . 1 1 1 1 1 . 1 1 1 1 1 . 1 1 1 1 1 1 1 . . . . 1
    |  . . 1 1 . . . 1 1 1 . . 1 . 1 . 1 . . . . . 1 . 1 . . 1 . 1 . . . . .
    |  . . . . . . . . . . . . . . . . . . . . . . . . . . . . . . . . . . . . .
  0 |  . . . . . . . . . . . . . . . . . . . . . . . . . . . . . . . . . . . . .
              pixel along profile
```

Along the boundary of the binary profiles the operation Intersect/No-Intersect is applied considering the following moving operators

For the first binary profile, 4 operators are used sequentially, the blue "1" corresponding to the pixel being filtered:

```
1 . .     1 . .     . . 1     . . 1
1 . .     1 . .     . . 1     . . 1
1 1 .     1 1 1     . 1 1     . 1 1
```

If there is an intersection (if the shape of one of the operator is entirely contained in the shape of the edge of the profile), the value of the pixel is increased by 1. If there is no intersection, the pixel is left untouched.

For the second binary profile, the following 4 operators are used:

```
1 1 .     1 1 1     1 1 1     . 1 1
1 . .     1 . .     . . 1     . . 1
1 . .     . . .     . . .     . . 1
```

In this case, the value of the pixel is decreased by 1 if there is an intersection. This is equivalent to the No-Intersect operation. The image is filtered by successively applying the Intersect and No-Intersect operations to all horizontal, vertical, diagonal and back-diagonal profiles in the image, in this order. This filter gives excellent visual results when applied to 8-bit radar images, removing most of the speckle while preserving sharp edges.